Numerical analysis of the frequency chirp in quantum dot semiconductor lasers

Numerical Analysis of the Frequency Chirp in Quantum-Dot Semiconductor Lasers

Mariangela Gioannini and Ivo Montrosset, *Member, IEEE*

***Abstract*—We present a numerical model for the analysis of the chirp dynamics of quantum-dot (QD) semiconductor laser under large signal current modulation. The model is based on the multipopulation rate equation formalism, and it includes all the peculiar characteristics of the active QD material such as the inhomogeneous broadening of the gain spectrum, the presence of an excited state confined in the QDs and the presence of nonconfined states due to the wetting layer and the barrier. In this paper the model is applied to the analysis of the chirp of two QD single-mode lasers emitting from the ground state and from the excited state, respectively. In order to make comparisons of the chirp in various operating conditions, we define some equivalent parameters for quantifying the adiabatic and transient contributions to the chirp. These parameters are then used to analyze the chirp as function of the bias current, of the modulation depth and of the modulation frequency. All the various simulation results show that the carrier accumulation in the QD states, poorly involved in the stimulated emission process and the carrier dynamics in these states, can cause a nonzero chirp under current modulation even for the ideal condition of zero linewidth enhancement factor (or α-parameter) at the laser threshold.**

***Index Terms*—Frequency chirp, quantum-dot (QD) semiconductor laser, semiconductor laser modeling.**

I. Introduction

QUANTUM-DOT (QD) semiconductor materials for laser diodes (QD-LDs) and optical amplifiers (QD-SOAs) have captured an increasing interest in the last ten years [1] thanks to the particular material properties obtained with the 3-D carrier confinement in the QD states. In an ideal QD material the gain spectrum is symmetric around the peak and, therefore, the linewidth enhancement factor (LEF) is expected to be zero at the peak gain wavelength. The QD material is therefore very promising for low chirp QD-LD that may be used in telecom applications. For this reason many experimental and theoretical works were dedicated to the measurement and calculation of the LEF in QD-LD and SOA [2]–[7]. The various experiments have, however, reported not only a nonzero LEF but also a wide range of measured values: from very small ones [8] to surprising high values [9]. In [4], it was demonstrated that the measured LEF in QD-SOA depends significantly on the measurement procedure; in [2], it was emphasized that the LEF measured below threshold from the amplified spontaneous emission spectrum is very different from the one obtained above threshold from the FM/AM ratio. Theoretical explanations for these results in apparent contrast were given in [10] and [7]: the above-threshold-measured LEF depends on the carrier filling and on the dynamics in the QD states that do not contribute to the stimulated emission process. Consequently the measured LEF above threshold is different from the one measured at threshold and depends on the operating conditions (i.e., bias current, modulation frequency, etc.). This behavior is the direct consequence of the complexity of the QD material: the carrier and photon dynamics can not be approximated, as in the bulk or quantum-well case, with a simple standard rate equation (SRE) system (i.e., one equation for carriers and one for photons [11]) but it is necessary to introduce a model based on a set of multipopulation rate equations (MPRE model [12]) for representing the carrier dynamics in the various QD confined states. The nonuniformity of QD dimensions, determined by the self-assembling growth process, causes an inhomogeneous broadening and an asymmetry of the gain spectrum. The primary consequence is that many of the conclusions derived from the analysis of the standard RE system are no more valid in the QD case. For example simple analytical calculations on the SRE system predict that when the LEF is zero at threshold, the laser chirp is zero as well [11], but this conclusion is no more valid for QD-LD and a more complex model has to be considered.

According to these observations the LEF parameter losses part of its significance in quantifying the chirp properties of QD devices and it is better to address the problem of the frequency chirp avoiding misleading strict correlations with the LEF. The phase dynamics of QD-SOA has been accurately studied in [5] and [3] from both theoretical and experimental point of view whereas only few experiments report chirp measurements of QD-LD [13], [14] and, to the best of our knowledge, the chirp properties of a single longitudinal mode QD-LD have never been theoretically analyzed. The purpose of this paper is to analyze through numerical simulations the chirp characteristics of QD-LD and show how the nonidealities of the QD material (i.e., inhomogeneous gain broadening, presence of several confined states in QDs and the wetting layer (WL), etc.) affect the chirp and push the laser far from chirp free operation.

The paper is organized as follows. In Section II, we present the equations of the numerical model used to the study of the static and dynamic characteristics of QD-LD [7] and in Section III we apply the model to the analysis of the frequency chirp of the directly modulated QD-LD. In particular, we propose some equivalent parameters that allow to identify the causes of nonzero chirp and to quantify the chirp in various operating conditions. Finally, in Section IV, we draw the conclusions.

Manuscript received March 20, 2007; revised May 31, 2007.

The authors are with Dipartimento di Elettronica, Politecnico di Torino, 10129 Torino, Italy (e-mail: mariangela.gioannini@polito.it; ivo.montrosset@polito.it).

Color versions of one or more of the figures in this paper are available online at http://ieeexplore.ieee.org.

Digital Object Identifier 10.1109/JQE.2007.904306

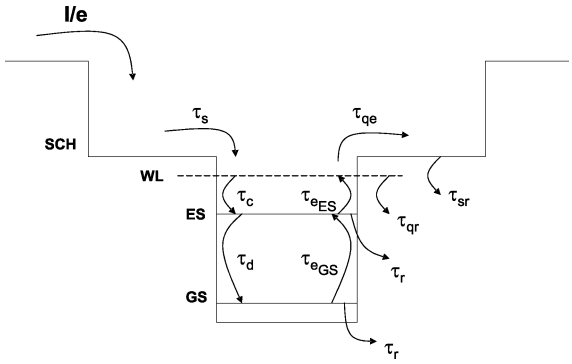

Fig. 1. Schematic of the energy band diagram of the QD SML active region. The carrier capture and escape rates from the various states are also indicated.

II. Numerical Model

The numerical model we use to analyze the chirp properties of single longitudinal mode QD-LD is based on the MPRE formalism presented in [7] and in [15]. Here we briefly summarize that model in order to define the notations. The model include the presence of a separate confinement heterostructure (SCH) state where carriers are injected [15], a WL state that acts as a common carrier reservoir [15], [16], [17], and the dot states coupled to the WL. The several dot states, due to the nonuniform size distribution of the QDs, lead to the inhomogeneous broadening of the gain [15], [16]. We have assumed that each QD has only two confined energy states, the ground state (GS) and the excited state (ES), the last one with a degeneracy equal to two due to the QD symmetry in the growth plane.

As in most of the papers that treat rate-equation models for QD materials [17], [15], [10], we consider only the electron dynamics assuming that the hole dynamics is so fast respect to the electrons that all the gain and spontaneous emission dynamical properties of the QDs are almost determined by the electron dynamics in conduction band. This approximation was quantitatively analyzed in [18] and [19]; the results show that the dynamics is mainly limited by the electron relaxations and the effect of the different electron and hole distribution are significant only at very low bias of the QD-LD. We consider this result a valid justification for the model we used and for the operation condition considered in this paper.

The carrier dynamics is schematized in Fig. 1. The carriers are injected in the SCH barrier with rate I/e, relax in the WL state with a rate $1/\tau_s$ or escape back in the barrier with the rate $1/\tau_{\rm qe}$. From the WL, they can be captured in the dots of different size. To include the effect of the size fluctuation of the QDs, we have divided the QD ensemble in several subgroups each characterized by an average energy of the ES, $E_{{\rm ES}m}$, and of the GS, $E_{{\rm GS}m}$, respectively. Therefore, the WL state acts as a common reservoir from which the carriers are captured in the ES of the mth subgroup with a rate $1/\tau_{cm}$ and from the ES to the GS with rate $1/\tau_{dm}$. The carriers also escape from the GS back in the ES with rate $1/\tau_{{\rm eGS}m}$ or from the ES back in the WL with rate $1/\tau_{{\rm eES}m}$. Carriers can also recombine with radiative and nonradiative processes from the SCH, from the WL, and from the various confined states with rates $1/\tau_{\rm sr}$, $1/\tau_{\rm qr}$, $1/\tau_{\rm r}$, respectively. The rate of photons emitted out of the cavity is $S_j/\tau_{{\rm p}_j}$, with $\tau_{{\rm p}_m}$ as the corresponding photon lifetime of the lasing mode.

The resulting rate equation system is as follows:

$$\frac{dN_s}{dt} = \frac{I}{e} - \frac{N_s}{\tau_s} - \frac{N_s}{\tau_{\rm sr}} + \frac{N_q}{\tau_{\rm qe}} \tag{1}$$

$$\frac{dN_q}{dt} = \frac{N_s}{\tau_s} + \sum_m \frac{N_{{\rm ES}m}}{\tau_{{\rm e}_{{\rm ES}m}}} - \frac{N_q}{\tau_{\rm qr}} - \frac{N_q}{\tau_{\rm qe}} - \frac{N_q}{\tau_{\rm c0}} \sum_m (1 - P_{{\rm ES}m}) G_m \tag{2}$$

$$\frac{dN_{{\rm ES}m}}{dt} = \frac{N_q G_m (1 - P_{{\rm ES}m})}{\tau_{\rm c0}} + \frac{N_{{\rm GS}m}(1 - P_{{\rm ES}m})}{\tau_{{\rm e}_{{\rm GS}m}}} - \frac{N_{{\rm ES}m}}{\tau_{\rm r}} - \frac{N_{{\rm ES}m}}{\tau_{{\rm e}_{{\rm ES}m}}} - \frac{N_{{\rm ES}m}}{\tau_{d0}}(1 - P_{{\rm GS}m}) + \frac{c\Gamma}{n_{\rm r}} \sum_j g_{j m_{\rm ES}} S_j \,, \qquad m = 0\,,\, 1\,,\, \ldots\,,\, M-1 \tag{3}$$

$$\frac{dN_{{\rm GS}m}}{dt} = \frac{N_{{\rm ES}m}}{\tau_{\rm d0}}(1 - P_{{\rm GS}m}) - \frac{N_{{\rm GS}m}}{\tau_{\rm r}} - \frac{N_{{\rm GS}m}(1 - P_{{\rm ES}m})}{\tau_{{\rm e}_{{\rm GS}m}}} - \frac{c\Gamma}{n_{\rm r}} \sum_j g_{j m_{\rm GS}} S_j \,, \qquad m = 0\,,\, 1\,,\, \ldots\,,\, M-1 \tag{4}$$

$$\frac{dS_j}{dt} = \beta \frac{N_j}{\tau_{\rm r}} + \frac{c\Gamma}{n_{\rm r}} \sum_j (g_{j m_{\rm ES}} + g_{j m_{\rm GS}}) S_j - \frac{S_j}{\tau_{{\rm p}_j}}. \tag{5}$$

In the equation system (1)–(5), we have one rate-equation for the total number of carriers in the SCH (N_s), one rate-equation for the total carriers in the WL (N_q), and M rate-equations for the carriers in the various QD subgroups ($N_{{\rm ES}m}$ and $N_{{\rm GS}m}$). These equations are then coupled with the lasing photon rate (5); since we analyze here the behavior of a single longitudinal mode laser for telecom applications, we consider only one RE for the lasing photons (i.e., we have just one longitudinal photon mode indexed by j).

In (5), the first term on the right-hand side ($\beta\,(N_j/\tau_{\rm r})$) represents the rate of photons emitted by spontaneous emission coupled into the lasing mode. N_j is chosen as the carriers in the QD state, ES or GS, with transition energy closer to the lasing photon energy E_j. This means we assume for simplicity that only spontaneous recombination from the QD subgroup with recombination energy closer to E_j feeds the S_j density. This is an approximation because other QD groups can also give spontaneously emitted photons at E_j due to the homogeneous broadening [12]. However, in the laser case, the spontaneous emission term is quite negligible above threshold and our approximation can be acceptable.

In (5), the stimulated emission rate of photons is proportional to the gain calculated as the sum of the contributions from the various states (GS, ES) and the various QD populations at the mode recombination energy E_j. Therefore, the terms $g_{j m{\rm GS}}$ and $g_{j m{\rm ES}}$ in (3)–(5) are calculated as

$$g_{j m_{\rm GS}} = \mu_{\rm GS}\, C_{\rm g} N_{\rm D} \frac{|P^{\sigma}_{\rm GS}|^2}{E_{{\rm GS}m}}\, (2P_{{\rm GS}m} - 1) G_m B_{\rm cv}(E_j - E_{{\rm GS}m}) \tag{6}$$

$$g_{jm_{\rm ES}}=\mu_{\rm ES}C_{\rm g}N_{\rm D}\frac{|P^{\sigma}_{\rm ES}|^2}{E_{{\rm ES}m}}(2P_{{\rm ES}m}-1)G_mB_{\rm cv}(E_j-E_{{\rm ES}m}) \tag{7}$$

where $\mu_{\rm GS}=2$ and $\mu_{\rm ES}=4$ are the degeneracy of the GS and ES levels including the spin; $C_{\rm g}$ is a constant [7], $N_{\rm D}$ is the dot density, $|P^{\sigma}_{\rm GS,ES}|^2$ are the transition matrix elements of the GS and ES recombination [15], $P_{{\rm GS}m}$ and $P_{{\rm ES}m}$ are the filling probability of the GS and ES, G_m is the existence probability of the mth QD subgroup, $B_{\rm cv}(E-E_{\rm GS,ES}{}_m)$ is the Lorentzian homogeneous broadening function with width $\hbar\Gamma_{\rm hom}$ [15]. To calculate G_m we have assumed the QD size distribution to be Gaussian satisfying $\sum_m G_m=1$. From (6) and (7), we can therefore calculate the gain for the recombination at the energy E_m in any time instant t.

In (2)–(4), the capture times τ_{c0} and τ_{d0} are the average capture time from the WL to the ES and from the ES to the GS with the hypothesis that the final state is empty; the Pauli blocking terms that make the capture times actually dependent on the QD distribution and filling are explicitly included in (2)–(4). In the same equations we have neglected the Paoli blocking terms for the escape from the ES to WL and for the escape from the WL to the SCH because we assume the WL and SCH states are always weekly occupied [17] for the the current injection levels considered in this paper.

Furthermore, at room temperature and without stimulated emission the system must converge to a quasi-thermal equilibrium characterized by a Fermi distribution of the carriers in all the states. To ensure this convergence the carrier escape time are related to the carrier capture times as follows: $\tau_{{\rm e}_{{\rm GS}m}}=\tau_{d0}(\mu_{\rm GS}/\mu_{\rm ES})\,e^{(E_{{\rm ES}m}-E_{{\rm GS}m})/k_{\rm B}T}$, $\tau_{{\rm e}_{{\rm ES}m}}=(\mu_{\rm ES}\,N_{\rm D}/\rho_{{\rm WL}_{\rm eff}})\tau_{c0}e^{(E_{\rm WL}-E_{\rm ES})/K_{\rm B}T}$ with $m=0,1,\ldots,M-1$. For the escape time from the WL in the SCH we use $\tau_{\rm qe}=(\rho_{{\rm WL}_{\rm eff}}N_w/\rho_{\rm SCH}H_b)\tau_s e^{\Delta E_{\rm SCH,WL}/k_{\rm B}T}$ with $\rho_{{\rm WL}_{\rm eff}}$ the density of states per unit area in the WL and $\rho_{\rm SCH}$ the density of states per unit volume in the SCH. They are given by $\rho_{{\rm WL}_{\rm eff}}=(m_{{\rm e}_{\rm WL}}k_{\rm B}T/\pi\hbar^2)$ and $\rho_{\rm SCH}=2\big(2m_{{\rm e}_{\rm SCH}}\pi k_{\rm B}T/\hbar^2\big)^{3/2}$.

In the above expressions N_d is the density of QD per unit area, N_w is the number of QD layers and H_b is the total thickness of the SCH, From the expression of $\tau_{{\rm e}_{ESn}}$ we see that the carrier escape time from the ES is dependent on the ratio between the number of available states in the QDs and in the WL; it has been shown that this ratio influences significantly the laser dynamics [20], [21].

In order to study also the phase fluctuations of the lasing mode we include in our model the calculation of the refractive index variation due to changes of the carrier density in the QDs, in the WL and in the SCH. The variation of the refractive index at the lasing mode energy E_j is given by the sum of two contributions: the term linked, through the Kramers-Kroning relation, to the gain variation ($\Delta n_{\rm QD}$) and the term caused by the free-carrier accumulation in the two dimensional WL and the 3-D SCH (plasma effect, $\Delta n_{\rm plasma}$) [22]. The expressions of these two terms are calculated as follows:

$$\Delta n_{\rm QD}(E_j)=\Gamma\frac{\hbar\,c}{2\,E}C_{\rm g}N_{\rm D}\sum_k\sum_m\mu_k\frac{|P^{\sigma}_k|^2}{E_k}\times(2P_{k_m}-1)G_mD_{\rm cv}(E_j-E_{k_m}). \tag{8}$$

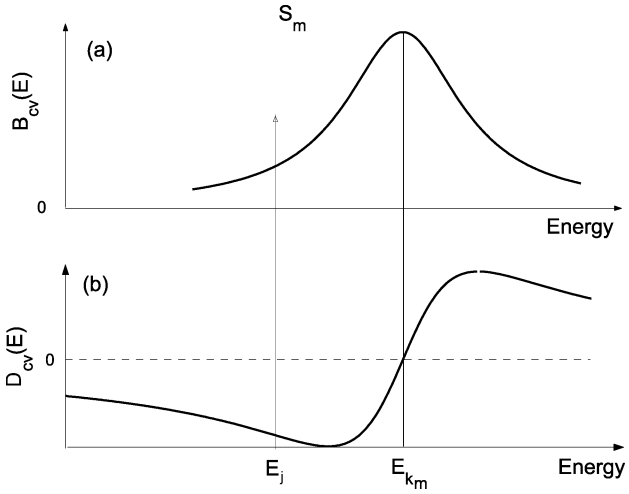

Fig. 2. Homogenous broadening functions of (a) the gain $B_{\rm cv}(E-E_{k_m})$ and (b) of the refractive index variation, $D_{\rm cv}(E-E_{k_n})$.

where the index k stays for the GS or ES transition; $D_{\rm cv}(E)$ is the homogenous broadening function of the refractive index spectrum, it is given by

$$D_{\rm cv}(E_j-E_{k_m})=\frac{\frac{(E_j-E_{k_m})}{\pi}}{(E_j-E_{k_m})^2+(\hbar\Gamma_{\rm hom})^2}. \tag{9}$$

The free-carrier contribution is given by

$$\Delta n_{\rm plasma}(E_j)=\Gamma_{\rm SCH}K_{\rm plasma}\frac{\Delta N_s}{E_j^2}+\Gamma_{\rm WL}K_{\rm plasma}\frac{\Delta N_q}{E_j^2} \tag{10}$$

where $\Gamma_{\rm SCH,WL}$ is the optical confinement factor in the SCH and WL and $K_{\rm plasma}=-\hbar^2e^2/2\varepsilon_0n_{\rm r}m^*_{\rm e}$.

The frequency fluctuation of the lasing mode is then given by

$$\nu(t,E_j)=-\frac{E_m}{2\pi\hbar n_{\rm g}}\Delta n_{\rm eff}(t,E_j) \tag{11}$$

where $\Delta n_{\rm eff}(t,E_j)$ is the total effective refractive index variation given by the sum of the terms in (8) and in (10).

From the stimulated emission term in (3) and (4), we see that the lasing photons S_j with energy E_j depletes also all the other carrier populations N_{k_m} with recombination energy E_{k_m} due to the homogenous broadening function $B_{\rm cv}(E_j-E_{k_m})$. For studying the phase dynamics of the lasing mode, it is important to note that a variation of the carrier density in the E_{k_m} state cause in turn a variation of the refractive index at the lasing energy E_j due to the $D_{\rm cv}(E_j-E_{k_m})$ broadening function. For clarity sake the broadening functions $D_{\rm cv}(E-E_{k_m})$ and $B_{\rm cv}(E-E_{k_m})$ are shown in Fig. 2; we observe that the width of the homogenous broadening function $D_{\rm cv}$ in Fig. 2(b) is much larger that the width of $B_{\rm cv}$. As a consequence any carrier variation in the QD states that do not take part to the stimulated emission process (because $B_{\rm cv}(E_j-E_{k_m})$ function is too small) can cause also a significant variation of the refractive index of the lasing mode E_j. This point is essential for modeling correctly the phase dynamics of QD-LD.

TABLE I
PARAMETERS OF THE QD MATERIAL AND LASER

QD MATERIAL PARAMETERS	LASER PARAMETERS
diffusion in SCH , $\tau_{\rm s}$=6 ns	active region length, $L_{\rm ca}$=900 μm
SCH recombination, $\tau_{\rm sr}$=4.5 ns	SCH thickness $H_{\rm b}$=90 nm
WL recombination, $\tau_{\rm qr}$=3 ns	WL thickness, $H_{\rm WL}$=1 nm
capture from WL to ES, $\tau_{\rm c0}$=1 ps	active region width w=10 μm
capture from ES to GS, $\tau_{\rm d0}$=7 ps	number of QD layers, $N_{\rm w}$=3
ES and GS recombination, $\tau_{\rm r}$=2.8 ns	active region volume, $V_{\rm A}$ =$2.2 \cdot 10^{-16} m^3$
energy separation SCH and WL state, 84 meV	QD density of QD per layer, $N_{\rm d}$=$5 \cdot 10^{10}\, cm^{-2}$
average energy separation WL and ES, 100 meV	QD density per unit volume $N_{\rm D}$ =$6.3 \cdot 10^{22}\, m^{-3}$
average energy separation ES and GS, 80 meV	SCH confinement factor, $\Gamma_{\rm SCH}$=0.2
average recombination energy from GS, $E_{\rm GS0}$=0.96 eV	WL confinement factor $\Gamma_{\rm WL} = 0.1$
average recombination energy from ES, $E_{\rm ES0}$=1.04 eV	QD optical confinement factor, Γ=0.06
homogeneous broadening $2\hbar\Gamma_{\rm k}$=20 meV at T=300K	internal modal loss, $\alpha_{\rm i}$=1 cm^{-1}
inhomogeneous broadening (Gaussian FWHM) 40 meV	spontaneous emission factor, β=10^{-4}
number of QD sub-groups M=15	

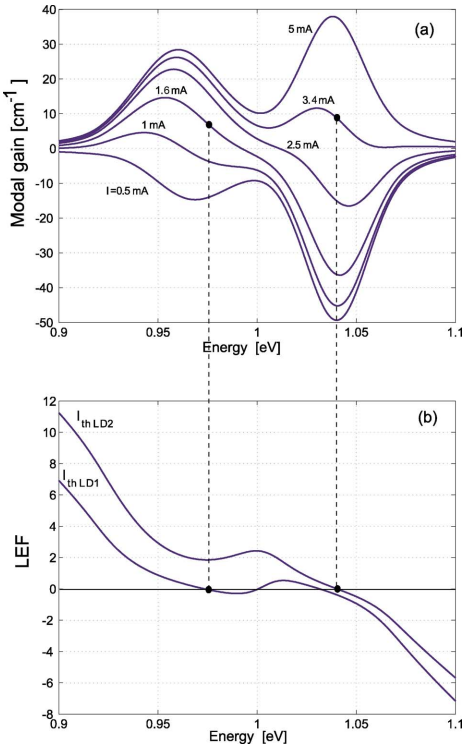

Fig. 3. (a) Modal gain spectra at various injection currents and (b) LEF spectra at the threshold currents of LD1 ($I_{\rm th,LD1} = 1.6$ mA) and LD2 ($I_{\rm th,LD2} = 3.4$ mA). The two dots in (b) indicate the lasing wavelength of LD1 and LD2 in the point of zero LEF; the dashed lines shows the corresponding threshold gain.

III. NUMERICAL RESULTS

In this section, we discuss the simulation results obtained applying the previous model to the analysis of single-mode QD-LD frequency chirp. Table I reports the parameters of the QD material and of the laser cavity under investigation. The QD material parameters where found in the literature and corresponds to those of an InAs–GaAs QD material system. The inhomogeneously broadened gain spectrum of the QD material is shown in Fig. 3(a); it has a GS peak at 0.96 eV and an ES peak at 1.04 eV. The LEF spectra of the QD material are shown in Fig. 3(b) and are calculated at two particular currents ($I_{\rm th,LD1} = 1.6$ mA and $I_{\rm th,LD2} = 3.4$ mA) selected as it will be justified in the following. These kind of spectra are similar to those could be obtained with experiments by amplified spontaneous emission measurements [2]. Fig. 3(b) demonstrates that even if the gain spectra are not symmetric due to inhomogeneous broadening and the presence of the ES, it is, however, possible finding at some injection currents a value of the emission energy for example, 0.973 eV at $I_{\rm th,LD1}$ and 1.04 eV at $I_{\rm th,LD2}$, see Fig. 3(b) where the LEF is null. At these zero-LEF energies, the total variation of the refractive index respect to the bias points is null because the positive contribution to the refractive index variation due to recombination with energies lower than the zero-LEF energy is exactly compensated by the negative contribution due to recombination with energies higher than the zero-LEF energy. This analysis confirms that, even in presence of inhomogeneous gain broadening and ES, the QD material can give a LEF equal to zero for some range of current injection. We have, however, observed that this condition does not imply chirp free operation when we work with a LD with zero-LEF at threshold. The purpose of this paper is to analyze the chirp properties of QD-LD focusing on the large signal operation. The small signal analysis was already reported in [10] for a GS emitting laser and in [7] for GS and ES emitting lasers. To focus exclusively on the chirp properties we have chosen two particular devices: a QD single-mode laser diode emitting from the GS (LD1) and another one emitting from the ES (LD2) both with zero LEF at their threshold currents, $I_{\rm th,LD1} = 1.6$ mA and $I_{\rm th,LD2} = 3.4$ mA.

This section is organized as follows: we first present the property of the frequency chirp of the directly modulated lasers and we analyze how the chirp depends on the working conditions (bias current, modulation depth, modulation frequency). We then analyze the chirp under nonreturn-to-zero (NRZ) modulation calculating the optical spectrum of the lasing mode.

A. Chirp Analysis

To analyze the chirp characteristics we have polarized both lasers at 25 mA and we have modulated them with a large signal sinusoidal current at 2.5 GHz. This modulation frequency is in both cases inside the -3 dB intensity modulation (IM) bandwidth of the devices (3.5 GHz for LD1 and 5.8 GHz for LD2). These IM bandwidths are rather small because the working wavelengths of LD1 and LD2 and the design of the cavity were not optimized to get the maximum IM bandwidth [23] but to

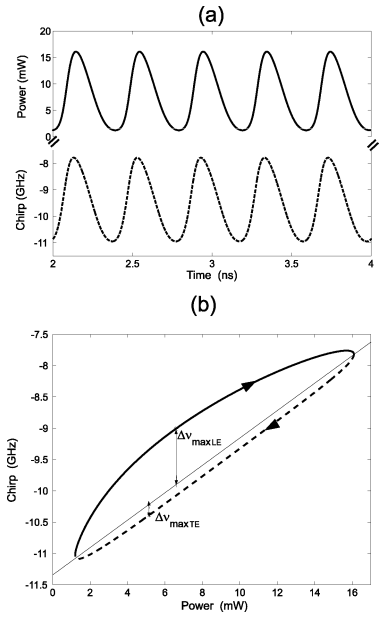

Fig. 4. (a) Power and frequency variation of the lasing mode in LD1 under large signal sinusoidal modulation at 2.5 GHz. (b) Representation of the chirp in the power-frequency plane ("fish diagram"). The straight line in (b) reports the adiabatic contribution; it is obtained connecting the two point of minimum and maximum of the power were $dP/dt = 0$. We indicate the point of maximum deviation ($\Delta\nu_{\max \mathrm{LE}}$ and $\Delta\nu_{\max \mathrm{TE}}$) of the chirp from the adiabatic part on the leading edge (solid line) and trailing edge (dashed line) of the power pulse. The two arrows on the curve indicates the time evolution.

have zero LEF at the laser threshold. We modulate first LD1 with a peak-to-peak current $I_{\mathrm{pp}} = 44$ mA. In Fig. 4(a), we show the output power and the frequency chirp of the lasing mode versus time; the figure evidence that even if we have zero LEF at threshold, the resulting chirp of the modulated LD is not null. In Fig. 4(b) we plot the power and the chirp of Fig. 4(a) in the power-frequency plane. This kind of representation ("fish diagram") was presented in [3] for the analysis of the chirp in quantum dash semiconductor amplifiers and we found it very useful to compare various simulation results and also for defining some equivalent parameters useful for the analysis of the chirp above threshold.

It is well known from the analysis of the SRE applied to bulk and quantum-well lasers [11] that the frequency chirp $\nu(t)$ can be written as

$$\nu(t) = \frac{\alpha}{4\pi}\left[\frac{1}{P(t)}\frac{dP(t)}{dt}\right] + k_a P(t) + \nu_{\mathrm{th}} \qquad (12)$$

where ν_{th} is the frequency deviation at the threshold respect to the cold cavity resonance and $P(t)$ is the total output power; α is the LEF at the laser threshold and k_a is a coefficient that is proportional to the LEF and depends on the gain saturation [11, eq. (5.96)]. The first two terms in the right-hand side of (12) represent, respectively, the transient contribution to the chirp (proportional to the power variation) and the adiabatic contribution (proportional to the power).

From the simulation results in Fig. 4, it is clear that expression (12) can not be used in the QD case for predicting the chirp characteristics reported in Fig. 4; indeed, if we use in (12) the standard parameters defined in [11, eq. (5.96)] the transient chirp would be null because we have zero LEF at threshold. We have also observed that it is not possible to fit the "fish" diagram defining in (12) an equivalent α (different from the threshold value), because the fitting would be possible only in a limited number of cases. This means that we can not use α as a constant in (12), but it should depend on the $P(t)$. However, we can still use expression (12) to study the chirp under the following considerations.

1) The slope of the "fish" diagram (straight line in Fig. 4(b) gives the adiabatic chirp quantified by the parameter k_a. The straight line is obtained connecting in the graph the two points where the power is minimum and maximum; in these point we have $dP/dt = 0$ and, therefore, zero transient contribution.
2) The deviation from the straight line in Fig. 4(b) is the transient contribution to the chirp that can be written as $\Delta\nu_{\mathrm{transient}}(t) = \nu(t) - k_a P(t) - \nu_{\mathrm{th}}$. We calculate for the leading edge (LE) and trailing edge (TE) of the power pulse the maximum transient contribution and then we define an equivalent LEF for the two edges ($\alpha_{\mathrm{LE,TE}}$) as

$$\alpha_{\mathrm{LE,TE}} = 4\pi \frac{\max\{\Delta\nu_{\mathrm{transient}}(t)\}|_{\mathrm{LE,TE}}}{\frac{1}{P(t)}\frac{dP(t)}{dt}\Big|_{\mathrm{LE,TE}}}. \qquad (13)$$

3) In the following, we will use the parameters k_a and $\alpha_{\mathrm{LE,TE}}$ to quantify the adiabatic and transient chirp in any operating condition.

For the example reported in Fig. 4 we have obtained $k_a = 0.21$ GHz/mW, $\alpha_{\mathrm{LE}} = 0.37$ and $\alpha_{\mathrm{TE}} = 0.17$. The values of the equivalent LEF are comparable with those obtained by chirp measurements of QD-LD in [14]; we have also two different values for the LE and TE as measured in [3]. To better understand which are the main mechanisms that cause a nonzero chirp above threshold, we have calculated the separate contributions to $\Delta\nu(t)$ due to the carrier variation in the QD GSs with emission energy lower then the lasing energy (we call it red GS contribution), in the QD group with emission energy equal to the lasing energy (lasing contribution), in the QD GS with emission energy higher than the lasing energy (blue GS contribution), in the ES (ES contribution). For each of these contributions we have then evaluated the equivalent parameters k_a and $\alpha_{\mathrm{LE,TE}}$; the results are summarized in Table II. The plasma term in Table II indicates the contribution due to free-carrier accumulation in the WL and SCH states; it is practically null because the WL and SCH are in this case practically empty. This plasma contribution can become more relevant if the separation between the GS and the WL is reduced [10]. The table shows

TABLE II
SEPARATE CONTRIBUTIONS TO THE CHIRP PARAMETERS

	LD1			LD2		
	k_{a} [GHz/mW]	α_{LE}	α_{TE}	k_{a} [GHz/mW]	α_{LE}	α_{TE}
red	~ 0	-0.54	-0.47	0.02	-0.28	-0.6
blue	0.012	0.19	0.08	0.04	0.32	0.06
lasing	~ 0	~ 0	~ 0	~ 0	~ 0	~ 0
ES for LD1	0.19	0.65	0.48			
GS for LD2				~ 0	-0.02	-0.07
plasma	~ 0	~ 0	~ 0	~ 0	0.03	-0.08
total	**0.22**	**0.37**	**0.17**	**0.07**	**0.04**	**-0.7**

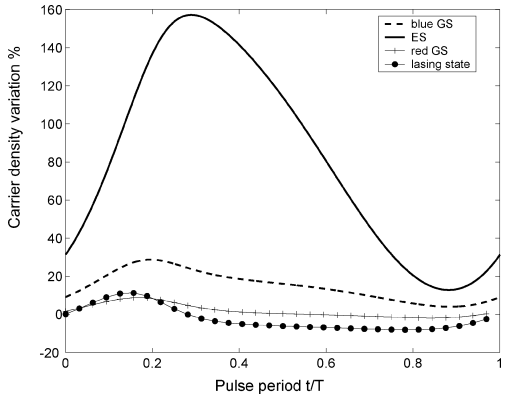

Fig. 5. Percentage variation of the carrier density respect to the threshold value in the various QD states of LD1 modulated with a sinusoidal current at 2.5 GHz with $I_{\rm pp} = 44$ mA and bias current $I_{\rm bias} = 25$ mA.

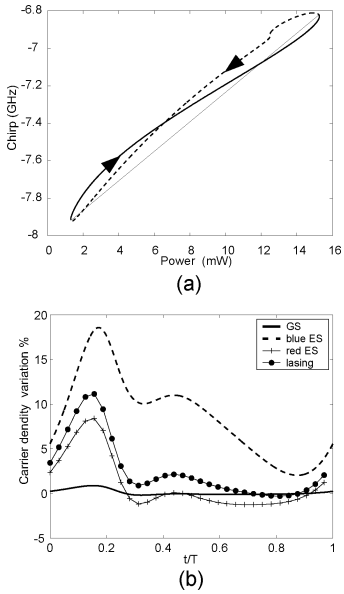

Fig. 6. (a) Frequency chirp as function of power ("fish diagram") of LD2 modulated at 2.5 GHz with $I_{\rm pp} = 35$ mA and bias current $I_{\rm bias} = 25$ mA. The solid straight line corresponds to the power pulse leading edge and the dashed line to the trailing edge with the arrows indicating the time evolution. The arrows on the curve indicate the time sequence. The straight line in (a) is the adiabatic contribution. (b) Corresponding variation of the carrier density respect to threshold in the various QD states.

that the adiabatic chirp is mainly due to the ES contribution; this is because the carrier density accumulated in the ES at $I_{\rm bias}$ can be significantly different from the threshold value. In [17], it was indeed shown that in a QD-LD the carrier density is not clamped at the threshold, but it continue to increase in those states that do not participate to the stimulated emission process. From Table II, we also observe that the equivalent LEF of the red GS is always negative whereas the equivalent LEF of the blue GS and ES is always positive. These contributions have always opposite signs because an increase/decrease of the carriers in the red states causes a negative/positive frequency shift of the lasing wavelength. On the contrary, an increase/deacrese of the carriers in the blue states and in the ES produces a positive/negative frequency variation. Even if these contributions have opposite signs they do not cancel each other as it happens at threshold, because the variation of the carrier occupation of the various states and the carrier dynamics in these states is different from the threshold. To better explain this point we report in Fig. 5 the variation of the carrier densities respect to their threshold values; we see that the carrier variation in the red GS and in the lasing states is rather small (less than 10%), the variation of the blue GS population is a bit larger (between 10% and 20%) but the variation of the ES carriers can be an order of magnitude higher. The higher energy states of the ES can indeed capture a lot of carriers that are only poorly depleted by the stimulated emission process. Table II also shows that the chirp due to the lasing QD group is practically zero even if the carrier variation is of the same order of the red GS. This is because the spectrum of the refractive index variation due to this group of dots has an odd symmetry around the lasing wavelength. This result shows that the chirp remains zero only if all the injected carriers are captured in the lasing states; this is not the case of a standard QD-LD because many other states (ES, GS in QD of other sizes) are available for the carriers.

The same analysis was repeated for LD2 with $I_{\rm pp} = 35$ mA chosen to have the same range of variation of the output power. The corresponding fish diagram is shown in Fig. 6(a); the Lemniscate-like shape of the diagram is due to the time delay between the power and the chirp variation (i.e., when the power starts decreasing, the chirp continue to increase). The variation of the carrier population respect to the threshold value is in Fig. 6(b) and the equivalent parameters for the various contributions to the chirp are in Table II. In this case the red/blue contributions are from those ES populations that have energy lower/higher than the lasing energy; for LD2 the GS contribution is due to the carrier accumulated in all the GS of the various QD subgroups. From Fig. 6(b), we see no variation of the GS population during a modulation period because the GS carriers remain practically clamped for the particular operating condition we have chosen. We can therefore predict that the contribution of the GS to the frequency chirp of LD2 is practically null. Table II shows that the adiabatic chirp k_a and the equivalent total LEF on the LE ($\alpha_{\rm LE}$) are now significantly reduced respect to LD1. On the LE the red and blue ES are filled at the same rate by the injected modulation current and the red negative contribution to $\alpha_{\rm LE}$ nearly compensate the blue positive one; furthermore the contribution from the WL and SCH is practically null. On the contrary the equivalent LEF on the TE ($\alpha_{\rm TE}$) is negative, higher than the value on the leading edge and it is mainly due to the carrier dynamics in the red ES. The red contribution dominates because on the pulse trailing edge the red ES is depleted by the power pulse with a rate higher than the blue ES . This behavior is particularly strong when we modulate with a frequency around the intensity modulation resonant frequency (estimated to be 2.9 GHz in this bias condition) and can not be observed in LD1 because the chirp is dominated by the carrier dynamics in the ES. We have seen that the value of $\alpha_{\rm TE}$ of LD2 is significantly dependent on the working conditions and can be reduced with a proper choice of the bias point (see Section III-B). In this example the plasma contribution is negligible as for LD1, but it may be more significant if the bias increases or the energy separation between ES and WL reduces because in these conditions the WL would accumulate a significant carrier density [6].

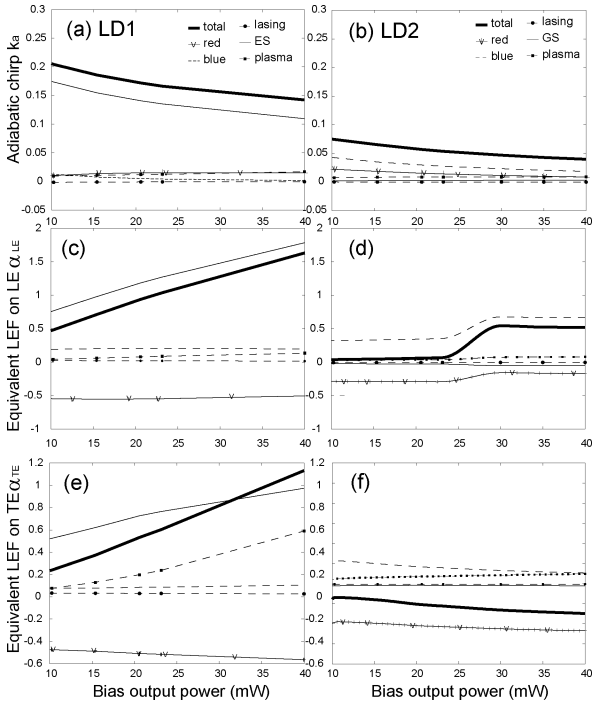

Fig. 7. Chirp parameters of (left) LD1 and (right) LD2 as function of the bias output power. For any bias point, the peak-to-peak modulation current has been chosen to guarantee an output power extinction ratio of 10 dB.

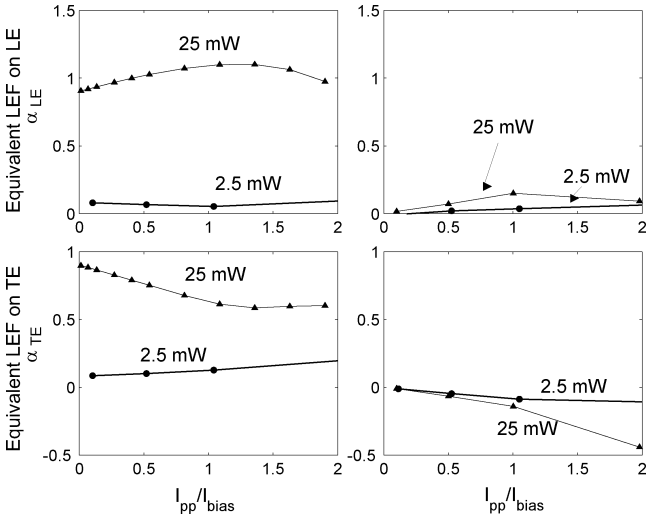

Fig. 8. Equivalent LEF parameters of (left) LD1 and (right) LD2 as function of the current modulation depth for two bias point corresponding to low (2.5 mW) and high (25 mW) output power.

B. Dependence of the Chirp on the Working Conditions

In the following, we analyze how the chirp of LD1 and LD2 modulated with a sinusoidal current depends on the working conditions such as the bias current, the peak-to-peak modulation current and the modulation frequency.

In the first example, we modulate both lasers with a large signal current at 2.5.GHz and we vary the bias current to get bias output power from 10 to 40 mW; for each bias point the peak-to-peak current is chosen to have an output power extinction ratio of 10 dB. In Fig. 7, we plot the extracted chirp parameters and the corresponding contributions from the various states as a function of the output power at the bias point. The figure demonstrates that for any bias current the chirp parameters [k_a in Fig. 7(a)–(b) and equivalent LEF in Fig. 7(c)–(f)] of LD1 are higher than in LD2. The equivalent LEF parameters ($\alpha_{\rm LE}$ and $\alpha_{\rm TE}$) always increase with increasing bias and in the case of LD1 the equivalent LEF reaches values even higher than one. A similar behavior has been experimentally observed in [2] through the small signal measurement of LEF from intensity over frequency modulation response and theoretically confirmed in [6] and [7]. From Fig. 7(c)–(d) and (e)–(f), we see that the mechanism responsible for the increasing LEF are different in the two lasers. In LD1 [Fig. 7(c) and (e)], the blue and red contributions remain practically constant with bias and the increasing contribution is only due to the ES. In LD1 the chirp is indeed dominated by the increased carrier occupation of the ES and of the WL because the carrier density of these states are not clamped by the stimulated emission of the photons. On the contrary in LD2 [Fig. 7(d) and (f)] the GS contribution is practically null and the increasing chirp is due to the nonexact compensation between the blue and red ES contributions. In the leading edge of LD2 [Fig. 7(d)] the two contributions nearly compensate at low bias; at higher bias, the blue contribution prevails on the red one. On the trailing edge [Fig. 7(f)] the behavior is opposite the red contribution is the dominant one.

As a second example, we analyze in Fig. 8 how the extracted equivalent LEF on the LE and TE depends on the modulation current. At this purpose LD1 and LD2 have been polarized to have 2.5 and 25 mW output power an we have varied the peak-to-peak modulation current from a very small value (one tenth the bias current as in a small signal regime) to a very large value (twice the bias current to operate in large signal regime). These results show that when we operate at low bias (output bias power of 2.5 mW) the equivalent LEF is very close to the zero threshold value and it starts increasing slightly if we move far from a small signal condition. In LD1 the equivalent LEF is strongly dependent on the bias point whereas it is practically unchanged with bias in LD2. For both lasers the dependence on the peak-to-peak modulation current is more pronounced when the output bias power is high (25 mW in Fig. 8).

Finally, in Fig. 9 we study the dependence of the equivalent LEF on the modulation frequency. The lasers are polarized to have the same output power of 23 mW. At these bias points the IM response -3-dB bandwidth was calculated equal to 4 GHz for LD1 and 5.2 GHz for LD2. We have varied the modulation frequency from 500 MHz to 7 GHz in the small ($I_{\rm pp} = 1/10 I_{\rm bias}$) and in the large ($I_{\rm pp} = I_{\rm bias}$) signal regime. Fig. 9(a) and (b) shows that the dependence of the chirp on the modulation frequency is more pronounced in large signal regime. The figures also show that the chirp depends more on the peak-to-peak modulation current if the modulation frequency is low whereas the equivalent LEF parameters in both small and large signal regime converge to the same value when we modulate at frequencies higher than the -3-dB bandwidth.

C. Chirp With NRZ Modulation

The last case we analyze is the behavior of the two lasers under NRZ modulation at 2 Gb/s with a periodic bit sequence

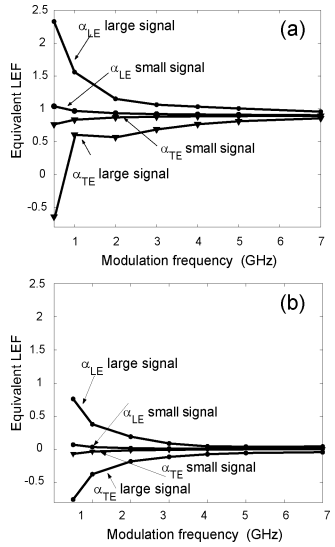

Fig. 9. Equivalent LEF parameters of LD1 and LD2 as function of the sinusoidal modulation frequency for small ($I_{\rm PP} = I_{\rm bias}/10$) and large ($I_{\rm PP} = I_{\rm bias}$) signal regime.

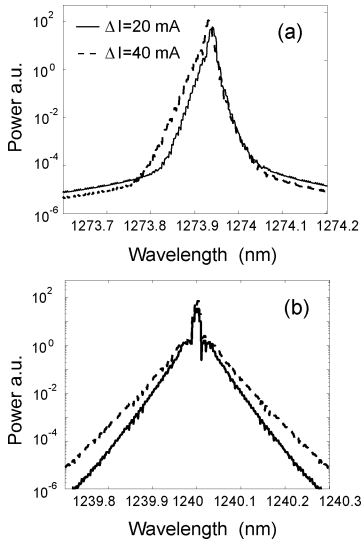

Fig. 10. Optical power spectrum of the lasing mode of (a) LD1 and (b) LD2 under NRZ modulation at 2 Gb/s.

1010.... In this analysis, the current pulse has a raised cosine shape and the current corresponding to the zero is chosen just above the threshold current. We analyze here two cases with current pulse $\Delta I = 20$ mA and $\Delta I = 40$ mA. To quantitatively compare the effect of the chirp in the various conditions, we have calculated the optical power spectrum of the lasing mode; the results are reported in Fig. 10. We see that increasing ΔI the spectrum of LD1 in Fig. 10(a) broadens only on the short wavelength side, whereas the spectrum of LD2 in Fig. 10(b) remains symmetric around the peak since it broadens equally on both sides. The broadening of the spectra in both cases is due to the excitation of the higher order harmonics caused by the squared current pulse. If the chirp is null or practically negligible the broadening is symmetric around the peak. If the chirp is not null with a predominant positive frequency shift the spectrum broadens on the short wavelength side, on the contrary it broadens on the red wavelength side if the chirp is dominated by a negative frequency shift. The broadening on the short wavelength side of the spectrum of LD1 [Fig. 10(a)] is another sign of the positive frequency chirp caused by the carrier accumulation in the ES. The comparison of Fig. 10(a) with Fig. 10(b) also evidences again the chirp of LD1 is higher than in LD2.

IV. Conclusion

In this paper, we have used a multipopulation rate-equation model to the analysis of the frequency chirp of two single-mode QD-LD modulated with a large signal current and emitting from the GS and from the ES, respectively. In order to stress the effect of the chirp we have chosen the laser cavity parameters to operate with a threshold current with zero LEF at the two lasing wavelengths. We have then presented a method for the analysis of the chirp based on the definition of some equivalent parameters that allow to quantify the adiabatic and transient contributions in various operating conditions. We have then analyzed how the two contributions vary with the bias current, the modulation depth and the modulation frequency. We have shown that the carrier accumulation in the QD states slightly involved in the stimulated emission process can cause a nonzero chirp above threshold. We have also observed that a QD-LD emitting from the GS gives a chirp significantly higher respect to a QD-LD emitting from the ES, because the carriers accumulated in the ES cause a significant refractive index variation also at the GS lasing wavelength.

References

[1] P. Bhattacharya, "Special issue on self-organized quantum dots," *J. Phys. D*, vol. 38, no. 13, Jul. 2005.

[2] A. Martinez, J.-G. Provost, A. Lemaitre, O. Gauthier-Lafaye, B. Dagens, K. Merghem, L. Ferlazzo, C. Dupuis, O. L. Gouezigou, and A. Ramdane, "Static and dynamic measurements of henry factor of 5-quantum dot layer single mode lasers emitting at 1.3 μm on GaAs," presented at the Conf. Lasers Electro-Optics, Long Beach, CA, May 2005, CThH1.

[3] D. Hadass, V. Mikhelashvili, G. Eisenstein, A. Somers, S. Deubert, W. Kaiser, J. Reithmaier, A. Forchel, D. Finzi, and Y. Maimon, "Time-resolved chirp in an InAs–InP quantum dash optical amplifiers operating with 10 Gbit/s data," *Appl. Phys. Lett.*, vol. 87, pp. 21104 1–3, 2005.

[4] S. Schneider, P. Borri, W. Langbein, U. Woggon, R. Sellin, D. Ouyan, and D. Bimberg, "Linewidth enhancement factor in InGaAs quantum-dot amplifiers," *IEEE J. Quantum Electron.*, vol. 40, no. 10, pp. 1423–1429, Oct. 2004.

[5] M. van der Poel, E. Gehrig, O. Hess, D. Birkedal, and J. Hvam, "Ultrafast gain dynamics in quantum dot amplifiers: Theoretical analysis and experimental investigation," *IEEE J. Quantum Electron.*, vol. 41, no. 9, pp. 1115–1124, Sep. 2006.

[6] A. U. S. Melnik and G. Huyet, "Phase-amplitude coupling of semiconductor quantum dot lasers," presented at the Conf. Lasers Electro-Optics, Munich, Germany, Jun. 2005, EA-14.

[7] M. Gioannini, A. Sevega, and I. Montrosset, "Simulations of differential gain and linewidth enhancement factor of quantum dot semiconductor lasers," *Opt. Quantum Electron.*, vol. 38, pp. 381–394, 2006.

[8] T. Newell, D. Bossert, A. Stintz, B. Fuchs, K. Malloy, and L. Lester, "Gain and linewidth enhancement factor in InAs quantum dot laser diodes," *IEEE Photon. Technol. Lett.*, vol. 11, no. 12, pp. 1527–1529, Dec. 1999.

[9] B. Dagens, A. Markus, J. Chen, J. Provost, D. Make, O. L. Gouezigou, J. Landreau, A. Fiore, and B. Thedrez, "Giant linewidth enhancement factor and purely frequency modulated emission from quantum dot laser," *IEE Electron. Lett.*, vol. 41, no. 6, pp. 323–324, Mar. 2005.

[10] S. Melnik, G. Huyet, and A. Uskov, "The linewidth enhancement factor α of quantum dot semiconductor lasers," *Opt. Exp.*, vol. 14, no. 7, pp. 2950–2955, Apr. 2006.

[11] L. A. Coldren and S. W. Corzine, *Diode Lasers and Photonic Integrated Circuits*. New York: Wiey, 1995.

[12] M. Sugawara, N. Hatori, H. Ebe, M. Ishida, Y. Arakawa, T. Akiyama, K. Otsubo, and Y. Nakata, "Modeling room-temperature lasing spectra of 1.3 μm InAs–GaAs quantum dot lasers: Homogeneous broadening of optical gain under current injection," *J. Appl. Phys.*, vol. 97, pp. 43523 1–8, 2005.
[13] H. Saito, K. Nishi, and S. Sugou, "Low chirp observed in directly modulated quantum dot lasers," *IEEE Photon. Technol. Lett.*, vol. 12, no. 10, pp. 1298–1300, Oct. 2000.
[14] N. Hatori, M. Ishida, H. Ebe, M. Sugawara, and Y. Arakawa, "Measurement and evaluation of chirp and linewidth ehnancement factor of a 1.3 μm quantum dot laser," in *Proc. Conf. Lasers Electro-Optics*, May 2004, vol. 1, p. 2.
[15] M. Sugawara, K. Mukai, Y. Nakata, H. Ishikawa, and A. Sakamoto, "Effect of homogeneous broadening of optical gain on lasing spectra in self-assembled $In_xGa_{1-x}As$/GaAs quantum dot lasers," *Phys. Rev. B*, vol. 61, no. 11, pp. 7595–7603, Mar. 2001.
[16] H. Huang and D. Deppe, "Rate equation model for nonequilibrium operating conditions in a self-organized quantum dot laser," *IEEE J. Quantum Electron.*, vol. 37, no. 5, pp. 691–698, May 2001.
[17] A. Markus, J. Chen, O. G.-L. J. Provost, C. Paranthoen, and A. Fiore, "Impact of intraband relaxation on the performance of a quantum-dot laser," *IEEE J. Sel. Topics Quantum Electron.*, vol. 9, no. 5, pp. 1308–1314, Sep./Oct. 2003.
[18] A. Markus, M. Rossetti, V. Calligari, J. X. Chen, and A. Fiore, "Role of thermal hopping and homogeneous broadening on the spectral characteristics of quantum dot lasers," *J. Appl. Phys.*, vol. 98, pp. 104506-1–8, 2005.
[19] A. Fiore and A. Markus, "Differential gain and gain compression in quantum dot lasers," *IEEE J. Quantum Electron.*, vol. 43, no. 3, pp. 287–294, Mar. 2007.
[20] D. Deppe and D. Huffaker, "Quantum dimensionality, entropy, and the modulation response of quantum dot lasers," *Appl. Phys. Lett.*, vol. 77, pp. 3325–3327, 2000.
[21] H. Dery and G. Eisenstein, "Self-consistent rate equations of self-assembly quantum wire lasers," *IEEE J. Quantum Electron.*, vol. 40, no. 11, pp. 1398–1409, Nov. 2004.
[22] S. Hegarty, B. Corbett, J. McInerney, and G. Huyet, "Free-carrier effect on index change in 1.3 μm quantum dot lasers," *IEE Electron. Lett.*, vol. 41, no. 7, pp. 416–418, Mar. 2005.
[23] M. Ishida, M. Sugawara, T. Yamamoto, N. Hatori, H. Erbe, Y. Kakata, and Y. Arakawa, "Theoretical study on high-speed modulation of Fabry-Perot and distributed feedback quantum dot lasers: K-factor limited bandwidth and 10 Gbit/s eye diagram," *J. Appl. Phys.*, vol. 101, pp. 13108-1–7, 2007.

Mariangela Gioannini was born in Italy in 1973. She received the Laurea degree in electronics engineering and the Ph.D. degree in electronic and communication engineering from Politecnico di Torino, Torino, Italy, in 1998 and 2002, respetively.

Since 2002, she has been with Dipartimento di Elettronica of Politecnico di Torino, first with a postdoctoral position and then since January 2005 as permanent Researcher. She was a Visiting Researcher at the Univesity of Bristol, Bristol, U.K., in 2001 and at the Fraunhofer Institut für Nachrichtentechnik, Heinrich-Hertz-Institut, Berlin, Germany in 2001 and 2002. Her research interests include modeling and characterization of semiconductor lasers and optical amplifiers. Since 2002, her research activity is focused on modeling of lasers and optical amplifiers based on semiconductor quantum-dot and quantum-dash materials.

Ivo Montrosset (M'92) was born in Aosta, Italy, in 1946. He received the Laurea degree in electronic engineering from the Politecnico di Torino, Torino, Italy, in 1971.

From 1972 to 1986, he was with the Politecnico di Torino. In 1986 he was appointed Full Professor at the Universita' di Genova, Genova, Italy. Since 1990, he has been Full Professor of optoelectronics at Politecnico di Torino. His main activities are in the field of guided wave-optics, solid-state and semiconductor lasers, and other related topics.

Mr. Montrosset is a member of IEEE LEOS and of OSA.